Enhancement of spin-orbit coupling and magnetic scattering in hydrogenated graphene

Shimin Cao [1,2] Chuanwu Cao [1,*] Shibing Tian,[3] and Jian-Hao Chen [1,2,4,5,†]

[1]*International Center of Quantum Material, School of Physics, Peking University, Beijing 100871, China*
[2]*Beijing Academy of Quantum Information Sciences, Beijing 100193, China*
[3]*Institute of Physics, Chinese Academy of Sciences, Beijing 100190, China*
[4]*Key Laboratory for the Physics and Chemistry of Nanodevices, Peking University, Beijing 100871, China*
[5]*Interdisciplinary Institute of Light-Element Quantum Materials and Research Center for Light-Element Advanced Materials,
Peking University, Beijing 100871, China*

Spin-orbit coupling (SOC) can provide essential tools to manipulate electron spins in two-dimensional materials like graphene, which is of great interest for both fundamental physics and spintronics application. In this paper, we report the low-field magnetotransport of *in situ* hydrogenated graphene where hydrogen atoms are attached to the graphene surface in continuous low temperature and vacuum environment. Transition from weak localization to weak antilocalization with increasing hydrogen adatom density is observed, indicating enhancing Bychkov-Rashba-type SOC in a mirror symmetry broken system. From the low-temperature saturation of phase breaking scattering rate, the existence of spin-flip scattering is identified, which corroborates the existence of magnetic moments in hydrogenated graphene.

I. INTRODUCTION

Spin-orbit coupling (SOC) is a relativistic effect which describes the mixing of electron spin and orbital motion. This process provides tools to the generation [1–3] and manipulation [4,5] of spin polarization in electron systems, which coincide with the main goal of spintronics. Graphene, a two-dimensional (2D) atomic layer of carbon, has the advantage of high stability and accessibility [6,7], high mobility and gate tunability [8], as well as long spin diffusion length [9,10], which makes it a suitable host for future spintronic applications. However, SOC in pristine graphene is expected to be weak due to relatively low electron velocity in carbon atoms [11]; furthermore, the first order of the atomic SOC vanishes due to the honeycomb arrangement of the carbon atoms [12]. Therefore, introducing SOC into graphene could provide an additional way to generate and manipulate spin, which has attracted extensive attention.

Hydrogenated graphene, e.g., graphene with hydrogen atoms covalently bonded to its surface, has been studied in several experiments recently [3,13–18]. Hydrogenated graphene is a complex system due to the randomness of the location of the hydrogen adatoms; therefore, it has rich physics. Great enhancement of the SOC up to three orders of magnitude and strong nonlocal transport up to room temperature due to spin Hall effect are reported [3]. Large negative magnetoresistance (MR) is frequently observed in hydrogenated graphene, which is found to be a hint of magnetic coupling between hydrogen adatoms [13,14]. Furthermore, hydrogen adatoms on bilayer graphene are found to energetically favor

a nondimer sublattice over a dimer sublattice, which is highly desirable for generating ferromagnetism [15].

In this paper, we report low-field ($B < 0.5$ T) MR of *in situ* hydrogenated graphene. We observed the transition between weak localization (WL) and weak antilocalization (WAL), which is tunable by hydrogen density and carrier density. The SOC strength extracted from the MR curves is found to be enhanced at high hydrogen density and low carrier density. Furthermore, the phase-breaking rate exhibits a saturation at low temperature, which is strong evidence in line with the scenario that hydrogen on graphene induces magnetic moments [19,20].

II. RESULT AND DISCUSSION

In situ doping is a powerful tool to introduce interactions to 2D materials. Various types of molecules, atoms, or ions can be deposited or bombarded on the sample surface to introduce different types of interactions, so that the strength of interactions can be almost continuously controlled by the amount of doping and can be detected via quantum transport, which is a great advantage comparing with other methods of introducing interactions like *ex situ* doping [21,22] or proximity effect [23,24] in heterostructures of graphene and transition metal ditellurides (TMDs), albeit the proximity effect has the potential to introduce ordered interactions.

In this experiment, hydrogen atoms were generated from a radio-frequency atom source, which flowed toward the sample with low kinetic energy and covalently bonded to the graphene surface [13]. Sample temperature was always kept at 5.8 K during hydrogen doping. The graphene sample was fabricated on SiO$_2$ substrate using a standard electron beam lithography technique and dry etched into Hall bar geometry. The sample was kept in an ultrahigh vacuum environment of up

---

*Currently in DQMP, University of Geneva.
†chenjianhao@pku.edu.cn
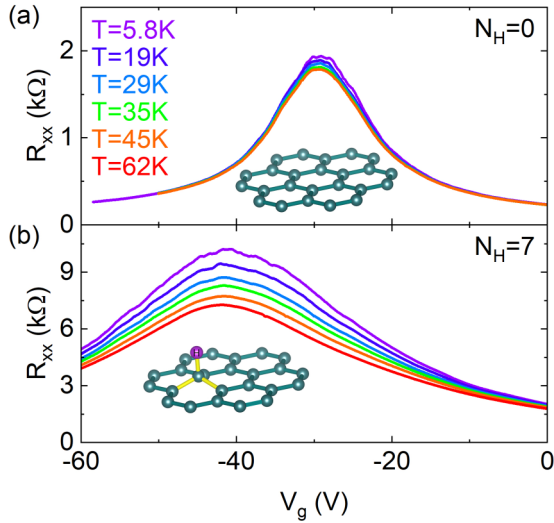
FIG. 1. Resistance as a function of back gate voltage V_g of (a) pristine and (b) hydrogenated graphene, respectively. N_H denotes hydrogenation rounds, e.g., $N_H = 7$ means after the seventh round of the hydrogenation process. Insets in the two panels are illustrations for the atomic structure of undoped and hydrogen-doped graphene.

to 10^{-9} Torr to reduce unwanted impurity absorption except during the doping process, when the graphene sample was exposed to a partial pressure of 10^{-2} Torr of hydrogen. The amount of hydrogen atoms on graphene can be controlled by the duration of the doping process (usually 5–10 s for each round of doping, 13 rounds of doping in this experiment) and quantitatively estimated from the conductance dependence on the carrier density of the sample after each hydrogenation round [13].

Figure 1 shows the resistance of (a) pristine ($N_H = 0$) and (b) hydrogenated ($N_H = 7$) graphene, respectively, where N_H stands for the round number of hydrogen adatom doping. Before hydrogenation, the resistance of graphene is smaller than the resistance quantum $R_Q = h/e^2$ with weak temperature dependence. Mobility of pristine graphene is found to be $4000 \, \mathrm{cm^2/Vs}$, which is a fair value for graphene on SiO$_2$ substrate. After hydrogenation, the Dirac point shifts toward the negative gate voltages, which means that hydrogen adatoms electron-doped graphene, consistent with a previous angle-resolved photo emission spectroscopy study [16]. Furthermore, with large hydrogen concentration, the resistance of hydrogenated graphene can be larger than R_Q near the Dirac point [13]. The resistivity of hydrogenated graphene is sensitive to temperature, but neither the thermal activation model nor the variable-range hopping model can be used to describe the resistivity vs temperature data even at the Dirac point (see Fig. S1 in the Supplemental Material [25]).

Next, we focus on the low-field ($B < 0.5$ T) magneto-transport properties of hydrogenated graphene. During our experiment, the hydrogen adatom density (n_H) increases monotonically from each round of hydrogenation. WL in graphene becomes apparent with a minimal number of n_H, and the WL signal increases with increasing n_H (see Fig. S2 in the Supplemental Material [25]), which is not surprising and can be understood as the enhancement of WL signal due to

increasing intervalley scattering from the hydrogen adatoms. What is more interesting is the evolution of the weak-field MR at higher n_H (from doping Round #6 to #11), which shows the systematic changes as a function of electron density (n_e) and n_H. Figure 2 shows MR of hydrogenated graphene at nine different combinations of n_e and n_H and at different temperatures. It can be seen that, in the high-n_e regime (e.g., the difference between gate voltage and Dirac point gate voltage $V_g - V_D \geqslant 40 \, \mathrm{V}$), increasing n_H simply suppresses the WL signal, as shown in Figs. 2(a)–2(f); in the low-n_e regime (e.g., $V_g - V_D \leqslant 10 \, \mathrm{V}$), on the other hand, increasing n_H causes a transition from WL to WAL. As will be shown in the discussion below, this is an observation of tunable WL-to-WAL transition in graphene where WAL is caused by factors other than the π Berry phase in the material. With increasing temperature, both WL and WAL signal decay rapidly, consistent with the dependence of such effects on phase coherent length of the electrons, which has strong temperature dependence.

Quantitatively, WL-WAL in graphene is caused by the interplay of various scattering mechanisms, usually including phase-breaking scattering rate τ_ϕ^{-1}, intervalley scattering rate τ_i^{-1}, and intravalley symmetry-breaking scattering rate τ_*^{-1} [26]. For hydrogenated graphene, since spin-orbit effect is known to be enhanced [3], it will also include Bychkov-Rashba (BR)-type SOC scattering rate τ_{BR}^{-1} or Kane-Mele (KM)-type SOC scattering rate τ_{KM}^{-1}. Thus, WL-WAL of graphene can be expressed as [26]

$$
\begin{aligned}
\frac{2\pi h}{e^2} \frac{\Delta\rho}{\rho^2} = & \, F\left(\frac{B}{B_\phi}\right) - F\left(\frac{B}{B_\phi + 2B_i}\right) - 2F\left(\frac{B}{B_\phi + B_*}\right) \\
& - 2F\left(\frac{B}{B_\phi + B_{BR} + B_{KM}}\right) \\
& + 2F\left(\frac{B}{B_\phi + 2B_i + B_{BR} + B_{KM}}\right) \\
& + 4F\left(\frac{B}{B_\phi + B_* + B_{BR} + B_{KM}}\right) \\
& - F\left(\frac{B}{B_\phi + 2B_{BR}}\right) + F\left(\frac{B}{B_\phi + 2B_i + 2B_{BR}}\right) \\
& + 2F\left(\frac{B}{B_\phi + B_* + 2B_{BR}}\right),
\end{aligned}
\tag{1}
$$

where $F(z) = \ln(z) + \psi(\frac{1}{2} + \frac{1}{z})$, $B_x = \frac{\hbar}{4De\tau_x} = \frac{\hbar}{4eL_x^2}$, $x = \phi, i, *, \mathrm{BR}, \mathrm{KM}$, ψ represents the digamma function, $D = v_F L_{mfp}/2$ is the diffusion constant determined by the Fermi velocity $v_F = 10^6 \, \mathrm{m/s}$ and mean free path $L_{mfp} = (\sigma/k_F)h/2e^2$. In order not to cause overfitting of the WL-WAL curves, it is essential to simplify Eq. (1) before fitting it to the experimental data.

The Elliot-Yafet (EY) type of spin relaxation describes the spin relaxation process in inversion symmetry preserving systems. Therein, energy of spin up and down states are still degenerate despite the existence of SOC. The spin up and down states are only slightly mixed by near-lying energy bands or energy levels [27]. It has been shown that an electron can flip its spin with certain probability at a momentum scattering event, leading to L_{EY} proportional to L_{mfp}. As for the Dyakonov-Perel (DP) case, the spin up and down states
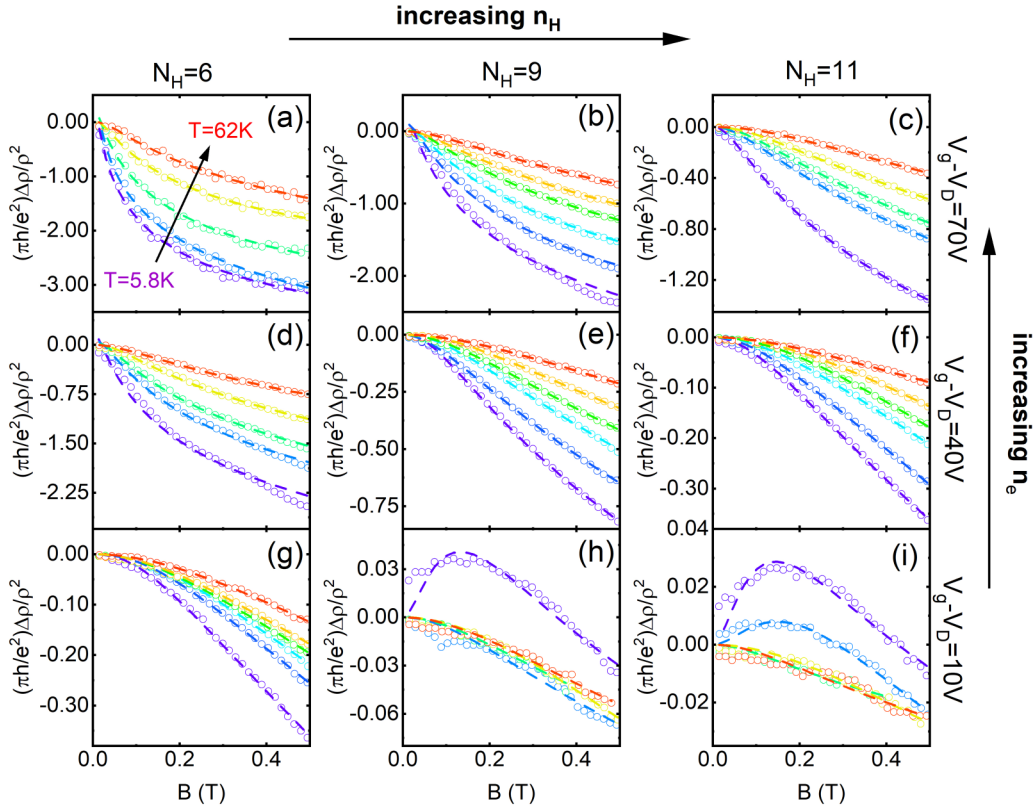
FIG. 2. Low-field ($B < 0.5$ T) magnetoresistance (MR) of hydrogenated graphene at various temperature T, carrier density n_e, and hydrogen density n_H. MR behavior of hydrogenated graphene shows transition from weak localization (WL) to weak antilocalization (WAL) at high n_H and low n_e (e.g., $V_g - V_D \leqslant 10$ V); WL suppression is observed at high n_H and high n_e (e.g., $V_g - V_D \geqslant 40$ V). MR of up to 9 T magnetic field can be found in Ref. [13]. The broken lines in the panels are fit to Eq. (2).

are split, forming an effective magnetic field which causes precession of electron spin between momentum scattering events [27]. In this case, L_{BR} is inversely proportional to L_{mfp}.

For hydrogenated graphene, decorated hydrogen atoms can only be on one side of the sample. Therefore, inversion symmetry is no longer held in the system. For hydrogen atoms absorbed on graphene surface, both theoretical calculation [28] and scanning tunneling microscopy experiments [18,29] have indicated the existence of spin-split states. These facts support the hydrogen-induced SOC should be of the DP type. Moreover, in our experiment, we observed the appearance of WAL signal, while the WL signal is broadening (see Fig. 2), which is also consistent with the scenario that Rashba-type SOC is introduced into the system, causing inversion symmetry breaking. Thus, all this evidence points to DP mechanism. Hence, the KM term does not enter the fitting. Furthermore, it has been shown that terms with the intravalley scattering rate usually provide small correction to the graphene WL signal [30,31]; therefore, related terms can also be dropped. With the above considerations, Eq. (1) becomes

$$\frac{2\pi h}{e^2}\frac{\Delta\rho}{\rho^2} = F\left(\frac{B}{B_\phi}\right) - F\left(\frac{B}{B_\phi + 2B_i}\right) - 2F\left(\frac{B}{B_\phi + B_{BR}}\right)$$
$$+ 2F\left(\frac{B}{B_\phi + 2B_i + B_{BR}}\right) - F\left(\frac{B}{B_\phi + 2B_{BR}}\right)$$
$$+ F\left(\frac{B}{B_\phi + 2B_i + 2B_{BR}}\right) \qquad (2)$$

As shown in Fig. 2, Eq. (2) fits to the magnetotransport data very well, and the resultant fitting parameters $B_x = \frac{\hbar}{4eL_x^2}$, where $x = \phi$, i, BR, can be extracted. Among these parameters, L_{BR} and L_ϕ are shown in Fig. 3 as a function of n_H [Figs. 3(a) and 3(b)], V_g [Figs. 3(c) and 3(d)], and temperature [Figs. 3(e) and 3(f)]. We shall discuss these two important parameters in detail in the following paragraphs.

First, the BR SOC scattering length L_{BR} is found to reduce for higher n_H [Fig. 3(a)], which strongly supports our assertion that single-sided hydrogenation of graphene enhances its overall Rashba SOC strength. Second, L_{BR} is also found to reduce as the Fermi level gets close to the Dirac point [Fig. 3(c)], which is consistent with another graphene hydrogenation experiment [3], except for the case of graphene/transition metal dichalcogenide heterostructure, where SOC strength is reported to slightly decrease toward the Dirac point [24,32]. In addition, the gate tunability of SOC in hydrogenated graphene is much higher than that in graphene/TMD heterostructure [24,32,33], which is essential for manipulating and utilizing the spin degree of freedom in graphene-based devices. It is worth noting that, with increasing n_H, L_{BR} and the momentum scattering length L_{mfp} are both decreasing; L_{BR} seems positively related to L_{mfp} (see Fig. S3 in the Supplemental Material [25]). This appears to contrast with the conventional expectation of the DP mechanism. We argue that stronger Rashba coupling leads to longer momentum mean free path only in ordered systems, e.g., that the introduction of Rashba coupling is applied uniformly to the whole sample. In the case of random
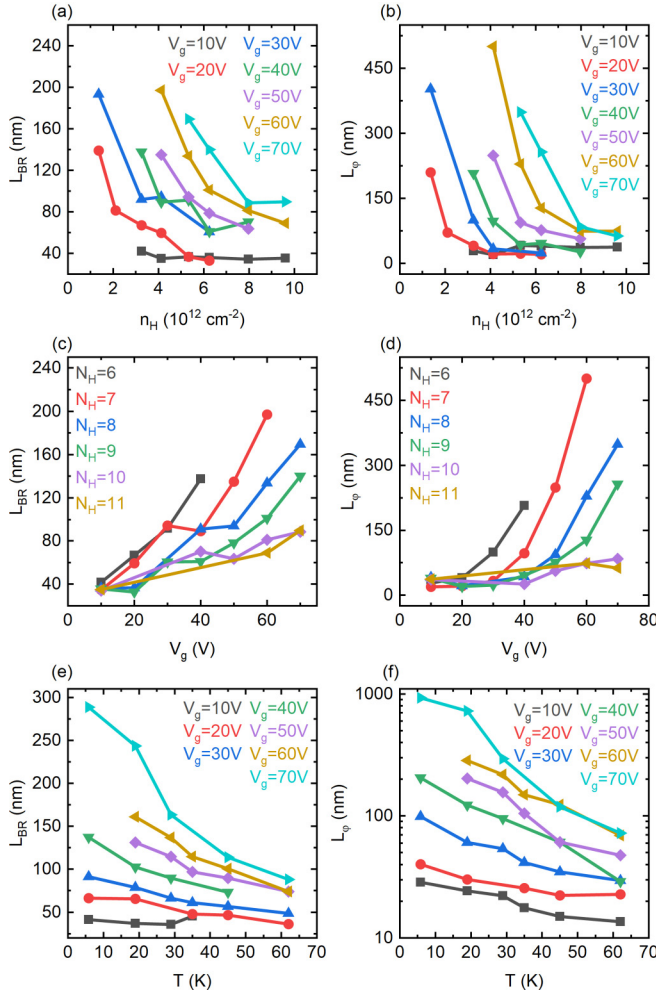
FIG. 3. Weak antilocalization (WAL) fitting results of hydrogenated graphene. (a), (c), and (e) The Bychkov-Rashba (BR) spin-orbit coupling (SOC) scattering length L_{BR} vs n_H, V_g, and T, respectively. (b), (d), and (f) The phase-breaking scattering length L_φ vs n_H, V_g, and T, respectively. (e) and (f) are taken from $N_H = 6$ data.

FIG. 4. T dependence and saturation of phase breaking rate τ_ϕ^{-1}. (a) Experimental τ_ϕ^{-1} vs T data (dots) and fitting to Eq. (3) (solid line). (b) and (c) Saturated phase-breaking rate τ_{sat}^{-1} vs n_H and V_g, respectively.

Rashba scattering, the introduction of Rashba coupling simultaneously increases momentum scattering due to the local and disordered nature of the interaction, thus strongly suppressing momentum scattering length (L_{mfp}). It has been shown [34] that, for random Rashba scattering, the DP mechanism can produce either DP-like or EY-like behavior. Thus, in this case, L_{BR} could have a proportional relationship with L_{mfp}. Two additional factors mentioned in the above paragraphs support the DP mechanism: (1) hydrogenation at the top surface of the graphene clearly breaks the mirror symmetry; (2) KM SOC will not induce WAL observed in the hydrogenated samples.

Now we turn to the discussion of L_ϕ, the phase coherence length. Here, L_ϕ shows similar behavior to L_{BR}, which indicates that phase-breaking scattering is enhanced with increasing n_H [Fig. 3(b)], decreasing n_e [Fig. 3(d)], or increasing temperature [Fig. 3(f)], which agrees with other works on WL-WAL in graphene [24,32,35]. The phase-breaking rate τ_ϕ^{-1} of graphene is calculated from $\tau_\phi^{-1} = D/L_\phi$, where $D = v_F L_{mfp}/2$ is the diffusion constant. It is known that the phase-

breaking rate in graphene can be described as [20,36]

$$\tau_\phi^{-1} = aT + bT^2 + \tau_{sat}^{-1}. \tag{3}$$

The first term (linear in temperature T) in Eq. (3) is attributed mainly to the electron-electron interactions of 2D electron gas in the diffusive regime [20,36–39], as well as the electron-phonon scattering process [38]; the second term ($\propto T^2$) in Eq. (3) is considered to arise from electron-electron interactions in graphene [20,36]. At low temperatures, τ_ϕ^{-1} should saturate to a constant term τ_{sat}^{-1} according to Eq. (3). Figure 4(a) plots the temperature dependence of τ_ϕ^{-1} for graphene after the ninth round of hydrogenation and at different V_g (different n_e). It is clear that τ_ϕ^{-1} at all carrier densities decreases and shows saturation behavior at low temperature.

The constant term τ_{sat}^{-1} in Eq. (3) for graphene with magnetic adatoms is found to be the spin-flip scattering rate τ_{sf}^{-1} [20], which can be described by the Nagaoka-Suhl formula [19,20,40]:

$$\tau_{sf}^{-1} = \frac{n_{mag}}{\pi \hbar N(E_F)} \frac{\pi^2 S(S+1)}{\pi^2 S(S+1) + \ln^2(T/T_K)}, \tag{4}$$

where n_{mag} is the density of magnetic impurities, S is the total spin of the magnetic impurities, which is taken as $\frac{1}{2}$ for hydrogen adatoms on graphene [41]. In addition, T_K is the Kondo temperature, which is defined as $k_B T_K = A \exp[-1/N(E_F)J]$, with $A = 10$ eV the cutoff energy, J the Kondo exchange energy, and $N(E_F) = 2\sqrt{n}/(\sqrt{\pi}\hbar v_F)$ the density of states at the Fermi level. Using the estimated hydrogen atom density [13] as n_{mag}, T_K is found to be $\ll 1$ K, which is consistent with our experimental observation. In the meantime, due to the small T_K, τ_{sf}^{-1} does not change much in the temperature range of this experiment (5.8–60 K). The n_H and n_e dependence of τ_{sat}^{-1} is plotted in Figs. 4(b) and 4(c), respectively. Here, τ_{sat}^{-1} increases with more hydrogen atoms absorbed on the graphene surface and decreases when the Fermi surface

of the graphene moves away from the Dirac point, which is consistent with the expectation of the Nagaoka-Suhl formula. This is important evidence showing that hydrogen adatoms on graphene are indeed magnetic and can induce spin-flip scattering.

For both spin-orbit scattering and spin-flip scattering, an interesting trend can be observed: adatom-related scattering seems to be stronger at lower charge carrier density. In other words, when carrier density is lower, the "effective hydrogen density" seems to be higher to give stronger physical effect, say SOC and magnetic scattering. This phenomenon can be understood in terms of screening effect by the conduction electrons. First, the Rashba scattering, like other scattering events (e.g., scattering from charged impurities or neutral scatterers), can be screened by the conduction electron [42]. Thus, a smaller density of states at the Fermi level (gate voltage closer to the $V_{\rm D}$) means weaker screening and thus stronger effective scattering. Specifically, due to the screening of charge carriers, impurity scattering in graphene develops Friedel oscillation. For $k_F r \gg 1$, the impurity-induced change of local particle density [43] $\delta n \propto \sin(2k_F r)/r^2$, where r is distance to the impurity and $k_F \propto \sqrt{\pi n_e}$ is the Fermi vector of graphene. The fast oscillation causes the impurity scattering to cancel out when we average the change of local carrier density all over the sample. Therefore, we can define an *effective radius* of an impurity to be $r_i \sim 1/k_F = 1/\sqrt{\pi n_e}$. When carrier density is lower, effective radius of the impurity is increased, leading to stronger SOC and magnetic scattering to charge carriers.

III. CONCLUSIONS

In summary, we have investigated low-field magneto-transport properties of *in situ* hydrogenated graphene and observed hydrogen density and carrier density tunable WL-to-WAL transition. By analyzing the low-field MR, we determined the strength of BR-type SOC can be efficiently tuned with hydrogen density and carrier density. From the temperature-dependent phase-breaking scattering rate, the saturation scattering rate is deduced and confirmed to be spin-flip scattering, which is important evidence for magnetic scattering induced by hydrogen adatoms on graphene.

[1] J. Liu, L. J. Cornelissen, J. Shan, B. J. van Wees, and T. Kuschel, Nonlocal magnon spin transport in yttrium iron garnet with tantalum and platinum spin injection/detection electrodes, J. Phys. D: Appl. Phys. **51**, 224005 (2018).

[2] T. S. Ghiasi, A. A. Kaverzin, P. J. Blah, and B. J. van Wees, Charge-to-spin conversion by the Rashba-Edelstein effect in two-dimensional van der Waals heterostructures up to room temperature, Nano Lett. **19**, 5959 (2019).

[3] J. Balakrishnan, G. K. W. Koon, M. Jaiswal, A. C. Neto, and B. Özyilmaz, Colossal enhancement of spin-orbit coupling in weakly hydrogenated graphene, Nat. Phys. **9**, 284 (2013).

[4] E. I. Rashba and A. L. Efros, Efficient electron spin manipulation in a quantum well by an in-plane electric field, Appl. Phys. Lett. **83**, 5295 (2003).

[5] Y. Kato, R. C. Myers, A. C. Gossard, and D. D. Awschalom, Coherent spin manipulation without magnetic fields in strained semiconductors, Nature (London) **427**, 50 (2004).

[6] Y. Hao, L. Wang, Y. Liu, H. Chen, X. Wang, C. Tan, S. Nie, J. W. Suk, T. Jiang, T. Liang, J. Xiao, W. Ye, C. R. Dean, B. I. Yakobson, K. F. McCarty, P. Kim, J. Hone, L. Colombo, and R. S. Ruoff, Oxygen-activated growth and bandgap tunability of large single-crystal bilayer graphene, Nat. Nanotechnol. **11**, 426 (2016).

[7] H. Zhou, W. J. Yu, L. Liu, R. Cheng, Y. Chen, X. Huang, Y. Liu, Y. Wang, Y. Huang, and X. Duan, Chemical vapour deposition growth of large single crystals of monolayer and bilayer graphene, Nat. Commun. **4**, 2096 (2013).

[8] C. R. Dean, A. F. Young, I. Meric, C. Lee, L. Wang, S. Sorgenfrei, K. Watanabe, T. Taniguchi, P. Kim, K. L. Shepard, and J. Hone, Boron nitride substrates for high-quality graphene electronics, Nat. Nanotechnol. **5**, 722 (2010).

[9] W. Han and R. K. Kawakami, Spin Relaxation in Single-Layer and Bilayer Graphene, Phys. Rev. Lett. **107**, 047207 (2011).

[10] W. Han, R. K. Kawakami, M. Gmitra, and J. Fabian, Graphene spintronics, Nat. Nanotechnol. **9**, 794 (2014).

[11] A. H. C. Neto, F. Guinea, N. M. R. Peres, K. S. Novoselov, and A. K. Geim, The electronic properties of graphene, Rev. Mod. Phys. **81**, 109 (2009).

[12] A. De Martino, R. Egger, K. Hallberg, and C. A. Balseiro, Spin-Orbit Coupling and Electron Spin Resonance Theory for Carbon Nanotubes, Phys. Rev. Lett. **88**, 206402 (2002).

[13] S. Cao, C. Cao, S. Tian, and J.-H. Chen, Evidence of tunable magnetic coupling in hydrogenated graphene, Phys. Rev. B **102**, 045402 (2020).

[14] B. R. Matis, F. A. Bulat, A. L. Friedman, B. H. Houston, and J. W. Baldwin, Giant negative magnetoresistance and a transition from strong to weak localization in hydrogenated graphene, Phys. Rev. B **85**, 195437 (2012).

[15] J. Katoch, T. Zhu, D. Kochan, S. Singh, J. Fabian, and R. K. Kawakami, Transport Spectroscopy of Sublattice-Resolved Resonant Scattering in Hydrogen-Doped Bilayer Graphene, Phys. Rev. Lett. **121**, 136801 (2018).

[16] R. Balog, B. Jørgensen, L. Nilsson, M. Andersen, E. Rienks, M. Bianchi, M. Fanetti, E. Lægsgaard, A. Baraldi, S. Lizzit,

Z. Sljivancanin, F. Besenbacher, B. Hammer, T. G. Pedersen, P. Hofmann, and L. Hornekær, Bandgap opening in graphene induced by patterned hydrogen adsorption, Nat. Mater. **9**, 315 (2010).

[17] K. M. McCreary, A. G. Swartz, W. Han, J. Fabian, and R. K. Kawakami, Magnetic Moment Formation in Graphene Detected by Scattering of Pure Spin Currents, Phys. Rev. Lett. **109**, 186604 (2012).

[18] H. González-Herrero, J. M. Gómez-Rodríguez, P. Mallet, M. Moaied, J. J. Palacios, C. Salgado, M. M. Ugeda, J.-Y. Veuillen, F. Yndurain, and I. Brihuega, Atomic-scale control of graphene magnetism by using hydrogen atoms, Science **352**, 437 (2016).

[19] F. Pierre, A. B. Gougam, A. Anthore, H. Pothier, D. Esteve, and N. O. Birge, Dephasing of electrons in mesoscopic metal wires, Phys. Rev. B **68**, 085413 (2003).

[20] X. Hong, K. Zou, B. Wang, S. H. Cheng, and J. Zhu, Evidence for Spin-Flip Scattering and Local Moments in Dilute Fluorinated Graphene, Phys. Rev. Lett. **108**, 226602 (2012).

[21] B. Grbić, R. Leturcq, T. Ihn, K. Ensslin, D. Reuter, and A. D. Wieck, Strong spin-orbit interactions and weak antilocalization in carbon-doped p-type GaAs/Al$_x$Ga$_{1-x}$As heterostructures, Phys. Rev. B **77**, 125312 (2008).

[22] M. Csontos, T. Wojtowicz, X. Liu, M. Dobrowolska, B. Jankó, J. K. Furdyna, and G. Mihály, Magnetic Scattering of Spin Polarized Carriers in (In,Mn)Sb Dilute Magnetic Semiconductor, Phys. Rev. Lett. **95**, 227203 (2005).

[23] T. Wakamura, F. Reale, P. Palczynski, S. Gueron, C. Mattevi, and H. Bouchiat, Strong Anisotropic Spin-Orbit Interaction Induced in Graphene by Monolayer WS$_2$, Phys. Rev. Lett. **120**, 106802 (2018).

[24] Z. Wang, D. K. Ki, H. Chen, H. Berger, A. H. MacDonald, and A. F. Morpurgo, Strong interface-induced spin-orbit interaction in graphene on WS$_2$, Nat. Commun. **6**, 8339 (2015).

[25] See Supplemental Material at http://link.aps.org/supplemental/10.1103/PhysRevB.104.125422 for the details of resistance near Dirac point, magnetoresistance of early hydrogenation rounds, and similar results from a second sample.

[26] H. Aoki and M. S. Dresselhaus, *Physics of Graphene* (Springer Science & Business Media, New York, 2013).

[27] P. Boross, B. Dóra, A. Kiss, and F. Simon, A unified theory of spin-relaxation due to spin-orbit coupling in metals and semiconductors, Sci. Rep. **3**, 3233 (2013).

[28] N. Leconte, D. Soriano, S. Roche, P. Ordejon, J. C. Charlier, and J. J. Palacios, Magnetism-dependent transport phenomena in hydrogenated graphene: from spin-splitting to localization effects, ACS Nano **5**, 3987 (2011).

[29] Y. Zhang, S.-Y. Li, H. Huang, W.-T. Li, J.-B. Qiao, W.-X. Wang, L.-J. Yin, K.-K. Bai, W. Duan, and L. He, Scanning Tunneling Microscopy of the π Magnetism of a Single Carbon Vacancy in Graphene, Phys. Rev. Lett. **117**, 166801 (2016).

[30] J. A. Elias and E. A. Henriksen, Electronic transport and scattering times in tungsten-decorated graphene, Phys. Rev. B **95**, 075405 (2017).

[31] V. I. Fal'ko, K. Kechedzhi, E. McCann, B. L. Altshuler, H. Suzuura, and T. Ando, Weak localization in graphene, Solid State Commun. **143**, 33 (2007).

[32] B. Yang, M.-F. Tu, J. Kim, Y. Wu, H. Wang, J. Alicea, R. Wu, M. Bockrath, and J. Shi, Tunable spin-orbit coupling and symmetry-protected edge states in graphene/WS$_2$, 2D Mater. **3**, 031012 (2016).

[33] T. Wakamura, F. Reale, P. Palczynski, M. Q. Zhao, A. T. C. Johnson, S. Guéron, C. Mattevi, A. Ouerghi, and H. Bouchiat, Spin-orbit interaction induced in graphene by transition metal dichalcogenides, Phys. Rev. B **99**, 245402 (2019).

[34] P. Zhang and M. Wu, Electron spin relaxation in graphene with random Rashba field: comparison of the D'yakonov-Perel' and Elliott-Yafet-like mechanisms, New J. Phys. **14**, 033015 (2012).

[35] Z.-M. Liao, B.-H. Han, H.-C. Wu, and D.-P. Yu, Gate voltage dependence of weak localization in bilayer graphene, Appl. Phys. Lett. **97**, 163110 (2010).

[36] D.-K. Ki, D. Jeong, J.-H. Choi, H.-J. Lee, and K.-S. Park, Inelastic scattering in a monolayer graphene sheet: a weak-localization study, Phys. Rev. B **78**, 125409 (2008).

[37] D. J. Bishop, R. C. Dynes, and D. C. Tsui, Magnetoresistance in Si metal-oxide-semiconductor field-effect transistors: evidence of weak localization and correlation, Phys. Rev. B **26**, 773 (1982).

[38] F. V. Tikhonenko, A. A. Kozikov, A. K. Savchenko, and R. V. Gorbachev, Transition between Electron Localization and Antilocalization in Graphene, Phys. Rev. Lett. **103**, 226801 (2009).

[39] F. V. Tikhonenko, D. W. Horsell, R. V. Gorbachev, and A. K. Savchenko, Weak Localization in Graphene Flakes, Phys. Rev. Lett. **100**, 056802 (2008).

[40] K. Sengupta and G. Baskaran, Tuning Kondo physics in graphene with gate voltage, Phys. Rev. B **77**, 045417 (2008).

[41] D. Soriano, N. Leconte, P. Ordejón, J.-C. Charlier, J.-J. Palacios, and S. Roche, Magnetoresistance and Magnetic Ordering Fingerprints in Hydrogenated Graphene, Phys. Rev. Lett. **107**, 016602 (2011).

[42] C. Jang, S. Adam, J.-H. Chen, E. D. Williams, S. D. Sarma, and M. Fuhrer, Tuning the Effective Fine Structure Constant in Graphene: Opposing Effects of Dielectric Screening on Short- and Long-Range Potential Scattering, Phys. Rev. Lett. **101**, 146805 (2008).

[43] Á. Bácsi and A. Virosztek, Local density of states and Friedel oscillations in graphene, Phys. Rev. B **82**, 193405 (2010).